RESEARCH ARTICLE
SPACE PHYSICS: MAGNETOSPHERIC PHYSICS

Earth and Planetary Physics
7: 631–639, 2023
doi: 10.26464/epp2023080

Scalings for the Alfvén-cyclotron instability in a bi-kappa plasma

YueQun Lou[1,2], Xing Cao[3*], MingYu Wu[1,2], BinBin Ni[3,4], and TieLong Zhang[1,2,4,5*]

[1]Shenzhen Key Laboratory of Numerical Prediction for Space Storm, Institute of Space Science and Applied Technology, Harbin Institute of Technology, Shenzhen 518055, China;

[2]Key Laboratory of Solar Activity and Space Weather, National Space Science Center, Chinese Academy of Sciences, Beijing 100190, China;

[3]Department of Space Physics, School of Electronic Information, Wuhan University, Wuhan 430072, China;

[4]Chinese Academy of Sciences Center for Excellence in Comparative Planetology, Hefei 230026, China;

[5]Space Research Institute, Austrian Academy of Sciences, Graz 8042, Austria

Key Points:

- The influence of kappa distributions on the Alfvén-cyclotron instability under different plasma conditions is investigated in detail.
- An analytic scaling formula for dimensionless maximum growth rates is derived.
- The fitted growth rates agree well with the solutions to kinetic theory for various sets of spectral indexes and high-temperature anisotropy A_{hp} and plasma beta β_{hp} values of hot protons.

Citation: Lou, Y. Q., Cao, X., Wu, M. Y., Ni, B. B., and Zhang, T. L. (2023). Scalings for the Alfvén-cyclotron instability in a bi-kappa plasma. *Earth Planet. Phys.*, *7*(6), 631–639. http://doi.org/10.26464/epp2023080

Abstract: The particle velocity distribution in space plasma usually exhibits a non-Maxwellian high-energy tail that can be well modeled by kappa distributions. In this study, we focus on the growth rates of the Alfvén-cyclotron instability driven by ion temperature anisotropy in a kappa plasma. By solving the kinetic linear dispersion equation, we explore the sensitivity of growth rates to the spectral index κ of a bi-kappa distribution under different plasma conditions, including a variety of plasma beta β_{hp} and temperature anisotropy A_{hp} values of hot protons. Furthermore, a concise, analytic scaling formula is derived that relates the dimensionless maximum growth rate to three independent variables: the spectral index and the plasma beta and temperature anisotropy of hot protons. Our results show that as the κ-value increases, the instability bandwidth narrows and the maximum growth rate increases significantly. For higher β_{hp} and A_{hp}, the maximum instability undergoes a sharp increase as well. When our fits of dimensionless maximum growth rates are compared with solutions to kinetic linear dispersion theory, the results generally exhibit good agreement between them. Especially under the circumstances of large κ-values and high β_{hp} and A_{hp}, the scalings of maximum growth rates primarily accurately model the numerical solutions. Our analytic expressions can readily be used in large-scale models of the Earth's magnetosphere to understand wave generation due to the Alfvén-cyclotron instability.

Keywords: Alfvén-cyclotron instability; kappa distribution; kinetic linear dispersion theory; scaling formula

1. Introduction

The Alfvén-cyclotron instability is driven by the temperature anisotropy of ions with $T_\perp/T_\parallel > 1$, where $T_\perp$ and $T_\parallel$ are perpendicular and parallel temperatures of ions with respect to the ambient magnetic field (Gary, 1993). Linear dispersion theory of the Alfvén-cyclotron instability indicates that the free energy from hot ions excites enhanced electric and magnetic fluctuations at frequencies below ion gyrofrequency with positive growth rates. The growth rates generally maximize at parallel propagation ($\boldsymbol{k}\times\boldsymbol{B}_0 = 0$, where $\boldsymbol{k}$ is the wave vector, and $\boldsymbol{B}_0$ is the ambient magnetic field; Cornwall, 1965). The enhanced electromagnetic fluctuations at a frequency below the ion gyrofrequency are often termed electromagnetic ion cyclotron (EMIC) waves (Liu KJ et al., 2010; Min K et al., 2016; Gary et al., 2017).

Many processes are capable of affecting the dynamic equilibrium of the magnetosphere (Lu HY et al., 2013; Ni B et al., 2016; Su ZP et al., 2016; Hao YQ et al., 2017; Yu YQ et al., 2022). Among these mechanisms, numerous studies have stressed the importance of EMIC waves to the magnetospheric particle dynamics. Via cyclotron resonant interactions, EMIC waves are capable of rapidly losing the radiation belt electrons, leading to electron dropout in the radiation belts and efficiently precipitating ring current protons into the loss cone, emitting proton auroras at subauroral latitudes (Cornwall et al., 1970; Thorne and Kennel, 1971; Summers and Thorne, 2003; Xiao FL et al., 2012; Cao JB et al., 2013; Ni BB et al., 2015; Ni B et al., 2016; Shprits et al., 2016; Su ZP et al., 2016; Cao X et al., 2017a, 2019, 2020a, 2023; Engebretson et al., 2018; Ma Q et al., 2019; Yue C et al., 2019; Yu J et al., 2020;

First author: Y. Q. Lou, louyuequn@hit.edu.cn
Correspondence to: X. Cao, cxing@whu.edu.cn
T. L. Zhang, Tielong.Zhang@oeaw.ac.at
Received 30 JUN 2023; Accepted 08 SEP 2023.
First Published online 26 SEP 2023.

Lou YQ et al., 2021). Moreover, EMIC waves can heat cold electrons and heavy ions and result in the scattering loss of central plasma sheet protons (Thorne and Horne, 1997; Lu Q et al., 2007; Zhang JC et al., 2010; Zhou QH et al., 2013; Liang J et al., 2014; Cao X et al., 2016; Chen H et al., 2018; Kitamura et al., 2018; Zhu MH et al., 2021). It has also been reported that by means of bounce-resonance, EMIC waves can transport near-equatorial mirror electrons to lower pitch angles (Shprits, 2009; Cao X et al., 2017b).

Estimating the resonant wave–particle interactions is vital for the understanding of magnetospheric particle dynamics, which requires accurate global distribution information on the wave properties. Typically, statistical models are used to provide global wave maps, which generally yield the averaged wave parameters at given locations and geomagnetic disturbed levels. However, many localized, transient features might be smoothed because of the nature of statistics. Recent studies have shown that observations can be quite different from the statistical value for a specific event (Meredith et al., 2014; Fu XR et al., 2016; Yu YQ et al., 2022). Therefore, a few studies explored inferring wave properties by using particle information and plasma conditions. This hypothesis was first applied to wave instability. For instance, Blum et al. (2009) modeled the instability of EMIC waves by linear dispersion theory with plasma data from the Los Alamos National Laboratory Magnetospheric Plasma Analyzer. Bortnik et al. (2011) scaled the saturation wave amplitude and saturation time as a function of hot proton density and thermal anisotropy. The excitation and propagation effects were further investigated by Kang N et al. (2021), which confirmed the importance of temperature anisotropy. Fu XR et al. (2016) expanded the scaling research to four-dimensional parameter space and derived a scaling formula that related the saturation EMIC wave amplitude to initial plasma conditions. Additionally, they built an analytic connection between the saturation wave amplitude and the maximum linear growth rate. Further, Gary et al. (2017) obtained scaling relations for the maximum growth rate, the corresponding real frequency, and the saturated fluctuating magnetic field energy density.

However, the scaling relations for the Alfvén-cyclotron instability are generally performed in a bi-Maxwellian plasma. In a variety of space plasmas, particle velocity distributions possess a non-Maxwellian high-energy tail that can be well fitted by the kappa distribution (Christon et al., 1988; Summers and Thorne, 1991; Livadiotis, 2015). Furthermore, it has been reported that the presence of a high-energy tail on the particle distribution would result in a modification of the wave dispersion relation and growth rates of the Alfvén-cyclotron instability (Xue S et al., 1996; Chaston et al., 1997; Xiao FL et al., 2007; Zhou QH et al., 2012; Cao X et al., 2020b). The scalings of the Alfvén-cyclotron instability in a kappa plasma still lack comprehensive study.

In the present study, we aim to yield scaling relations for Alfvén-cyclotron instability growth rates in a bi-kappa plasma by using linear dispersion theory. The outline of this work is organized as follows: We introduce the kinetic linear dispersion relation of the Alfvén-cyclotron instability in a kappa plasma in Section 2. In Section 3, we analyze the numerical results of the linear growth rates and derive analytic expressions for the scaling of dimensionless maximum growth rates as functions of the spectral index and the plasma beta and temperature anisotropy of hot protons. We discuss the results and summarize the conclusions in Section 4.

2. Kinetic Linear Dispersion Relation in a Bi-kappa Plasma

Space plasmas that possess a non-Maxwellian high-energy tail can be well modeled by the bi-kappa distribution function (Summers and Thorne, 1991; Xiao FL et al., 2007; Cao X et al., 2020b) with the form of

$$f_s\left(v_{\|},v_{\perp}\right)=\frac{n_s}{\pi^{3/2}}\frac{1}{\theta_{\|s}\theta_{\perp s}^2}\frac{\Gamma\left(\kappa+1\right)}{\kappa^{3/2}\Gamma\left(\kappa-1/2\right)}\left(1+\frac{v_{\|}^2}{\kappa\theta_{\|s}^2}+\frac{v_{\perp}^2}{\kappa\theta_{\perp s}^2}\right)^{-(\kappa+1)}, \quad (1)$$

where n_s is the number density of particle species s; κ is the spectral index of the kappa distribution; Γ is the gamma function;

and $$\theta_{\|s}=\left[\left(2\kappa-3\right)/\kappa\right]^{1/2}\cdot\left(T_{\|s}/m_s\right)^{1/2}$$

and $$\theta_{\perp s}=\left[\left(2\kappa-3\right)/\kappa\right]^{1/2}\cdot\left(T_{\perp s}/m_s\right)^{1/2},$$

respectively, are the parallel and perpendicular thermal speed with respect to the uniform ambient magnetic field, where $T_{\|s}$ and $T_{\perp s}$ are temperatures parallel and perpendicular to the ambient magnetic field, respectively, and m_s is the rest mass of particles. Note that the spectral index κ has a maximum value of infinity and a minimum value of 3/2 (Livadiotis, 2015). As the spectral index of the kappa distribution $\kappa\to\infty$, the distribution reduces to a Maxwellian distribution. Consequently, the kappa distribution is a generalization of the Maxwellian distribution.

The Alfvén-cyclotron instability growth rates from solutions of the kinetic linear dispersion equation maximize at waves propagating parallel or antiparallel to the magnetic field. Assuming that the space plasmas can be modeled by bi-kappa distributions, the linear dispersion equation for parallelly propagating electromagnetic waves (Summers and Thorne, 1991; Xiao FL et al., 2007; Cao X et al., 2020b) is defined by

$$1=\frac{\omega^2}{\kappa_t^2c^2}+\sum_s\frac{\omega_{ps}^2}{\kappa_t^2c^2}\left\{A_s+\left[\omega+A_s\left(\omega-\Omega_s\right)\right]\left(\frac{\kappa}{\kappa-\frac{3}{2}}\right)\left(\frac{\kappa-1}{\kappa}\right)^{3/2}\frac{Z_{\kappa-1}^*\left(\zeta_s\right)}{\kappa_t\theta_{\|s}}\right\}, \quad (2)$$

where $\omega=\omega_r+\mathrm{i}\gamma$ is the complex wave frequency, where the real part ω_r is the real frequency and the imaginary part γ is the growth rate; k_t is the wave number; c is the speed of light; ω_{ps} is the plasma frequency of particles denoted by $\omega_{ps}=\sqrt{n_sq_s^2/m_s\varepsilon}$, where ε is the vacuum dielectric constant and q_s is the particle charge; $A_s=T_{\perp s}/T_{\|s}-1$ is the temperature anisotropy; $\Omega_s=q_sB_0/m_s$ is the particle gyrofrequency; Z^* is the modified plasma dispersion function; and $\zeta_s=\left[\left(\kappa-1\right)/\kappa\right]^{1/2}\left(\frac{\omega-\Omega_s}{k\theta_{\|s}}\right)$.

3. Numerical Results

Following previous studies (e.g., Gary et al., 2017), we use a cold, isotropic component (denoted by subscript c) and a hot, anisotropic component (denoted by subscript hp) represented as kappa velocity distributions to model the proton distributions in the magnetosphere. A cold, isotropic component with $n_e=n_c+n_{hp}$, $T_e=T_c$ is adopted to ensure quasi-neutrality. The temperature of cold components is set to be $T_c=T_{\|hp}/3000$, $T_{\|hp}/T_c\gg1$ is

adopted to avoid the influence of cold protons, and the hot proton abundance is n_{hp}/n_e = 10%. In the initial condition, the temperature anisotropy of hot protons A_{hp} is set to be 2, and the plasma beta of hot protons $\beta_{hp} = 8\pi n_{hp}T_{\|hp}/B_0^2$ is 0.5.

Figure 1 shows Alfvén-cyclotron instability growth rates as a function of wave numbers for different spectral indexes κ (κ = 2, 3, 5, and Maxwellian distribution [$\kappa = \infty$], respectively), where the growth rates are normalized to the proton gyrofrequency and the wave numbers are normalized by a factor of Ω_p/v_A (where v_A is the Alfvén speed). Figures 1a–1d exhibit the results at A_{hp}= 1, 2, 3, and 4, respectively, and Figures 1e–1h exhibit the results at β_{hp}= 0.25, 0.50, 1.0, and 2.5, respectively. As shown in Figure 1, for an increasing spectral index κ, the upper limit of unstable wave numbers due to the Alfvén-cyclotron instability remains almost unaffected, whereas the lower limit rises to a higher wave number, resulting in a narrower instability bandwidth. The growth rates decrease slightly for an increasing κ-value near the lower limit of the instability bandwidth but immediately exhibit a reverse tendency of moderate enhancement for an increasing κ-value at a larger wave number. Furthermore, the maximum growth rates indicate a modest intensification as well with an increase in the spectral index. This intensification exaggerates as the temperature anisotropy of hot protons A_{hp} grows. Moreover, the growth rates increase sharply for a rising A_{hp}, with the maximum growth rates increasing by a factor of approximately 4–5 for all the κ-values investigated from A_{hp}= 1 to A_{hp}= 4. In addition, the lower (upper) boundary of the instability bandwidth expands to a lower (higher) wave number at a higher A_{hp}. However, the upper limit of the instability wave numbers still remains almost unchanged for different spectral indexes. As for the plasma beta of hot protons β_{hp}, similar to the temperature anisotropy, an increasing κ-value results in a broader bandwidth and a greater maximum growth rate. The increase in β_{hp} corresponds to a dramatic enhancement in growth rates, especially for the peak growth rates. The lower limit of the instability extends significantly to a smaller wave number. But the upper limit decreases slightly with an increasing β_{hp}, which is opposite with A_{hp}.

Figure 2 shows the ratio of maximum growth rates in a bi-kappa distribution to that in a bi-Maxwellian distribution $\gamma_m/\gamma_{m,M}$ (hereafter referred as the "dimensionless maximum growth rate") with the solutions to the linear dispersion relation represented by red dots as a function of the spectral index κ for different temperature anisotropy A_{hp} (Figures 2a–2d) and plasma beta β_{hp} values (Figures 2e–2h). The relation between dimensionless maximum growth rates and the spectral index exhibits a trend analogous to the inverse proportional function. As a consequence, we assume the functional form

$$\gamma_m/\gamma_{m,M} = 1 - h_1 \cdot \kappa^{-h_2}, \tag{3}$$

and the resulting values of the fitting parameters h_1 and h_2 are given in Table 1. Using the numbers in this table, we find that h_1 and h_2 can be well fitted as functions of A_{hp} and β_{hp} with the following functions:

$$h_1 = \varepsilon_1 A_{hp}^{\ \varepsilon_{11}} \beta_{hp}^{\ \varepsilon_{12}} + \varepsilon_{13}, \tag{4a}$$

$$h_2 = \varepsilon_2 A_{hp}^{\ \varepsilon_{21}} \beta_{hp}^{\ \varepsilon_{22}}. \tag{4b}$$

Further fits of the linear dispersion theory results to the forms of

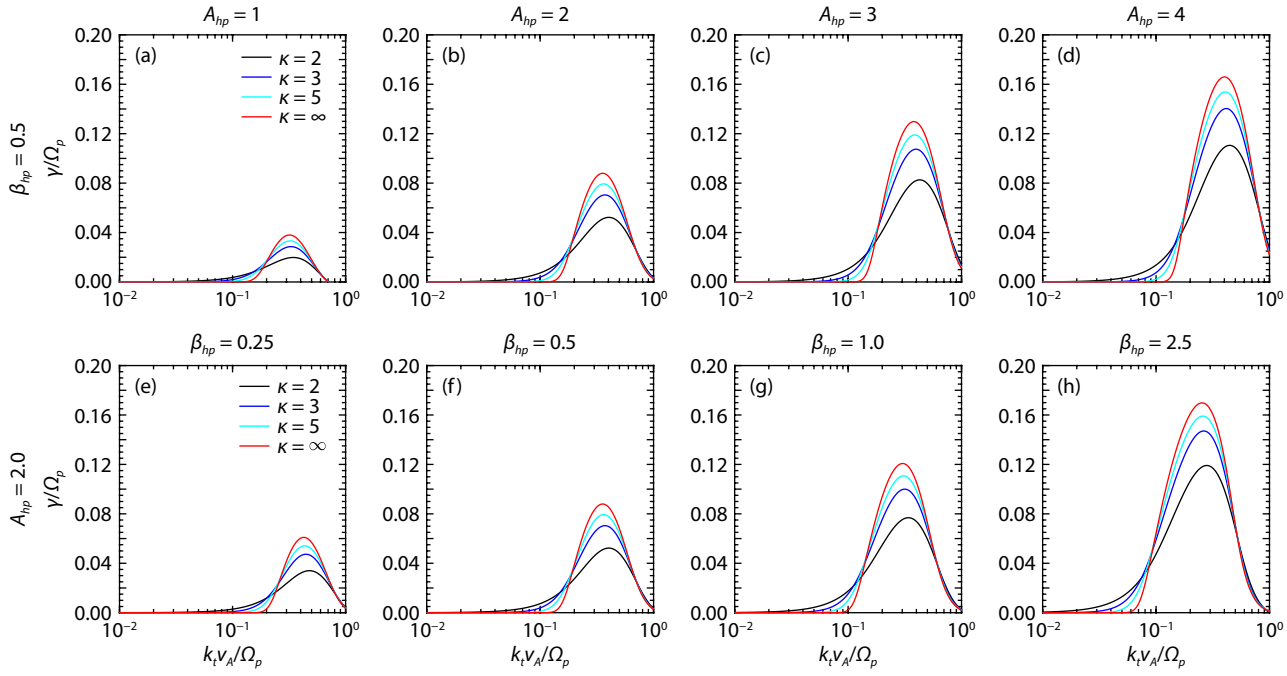

Figure 1. Linear growth rates normalized to the proton gyrofrequency as a function of wave numbers for the Alfvén-cyclotron instability in a plasma with a bi-kappa velocity distribution for (a–d) the four indicated temperature anisotropy values of hot protons (A_{hp}=1, 2, 3, and 4) at a fixed plasma beta β_{hp} = 0.5 and (e–h) the four indicated plasma beta values of hot protons (β_{hp} = 0.25, 0.50, 1.0, and 2.5) at a fixed temperature anisotropy A_{hp}= 2. The black, blue, cyan, and red curves represent growth rates for the spectral index κ = 2, 3, 5, and Maxwellian distribution ($\kappa = \infty$), respectively.

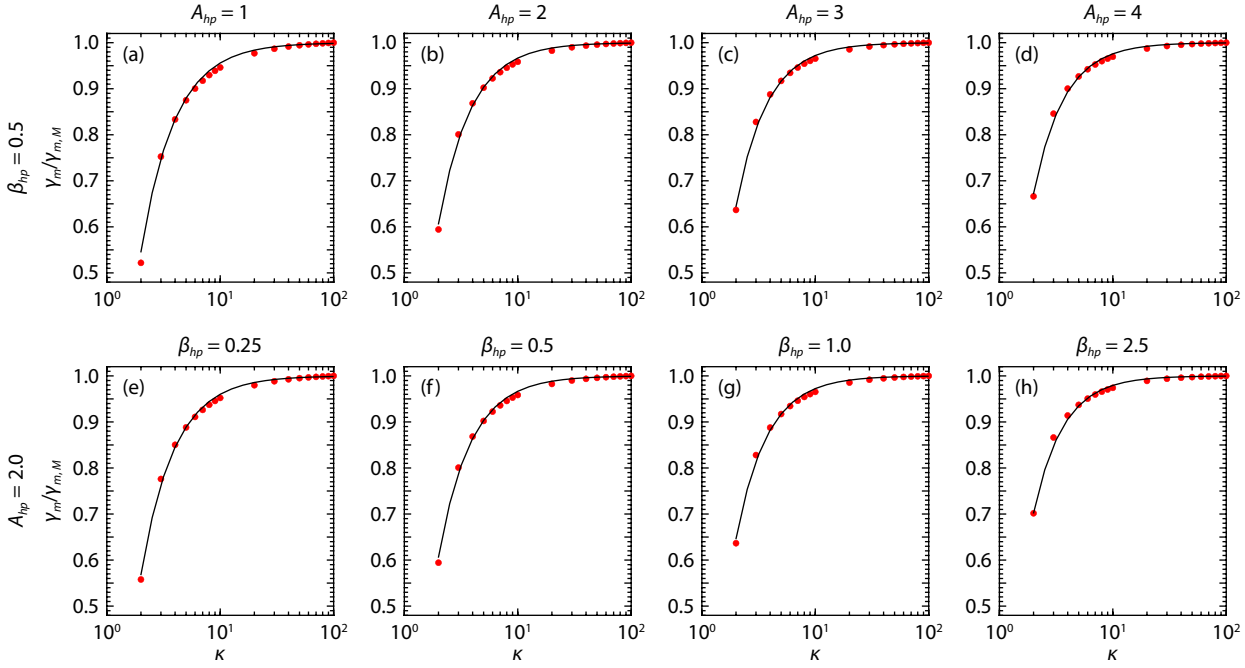

Figure 2. Ratio between maximum growth rates in a bi-kappa plasma and in a bi-Maxwellian plasma as a function of the spectral index κ for (a–d) the four indicated temperature anisotropy values of hot protons (A_{hp} = 1, 2, 3, and 4) at a fixed plasma beta β_{hp} = 0.5 and (e–h) the four indicated plasma beta values of hot protons (β_{hp} = 0.25, 0.50, 1.0, and 2.5) at a fixed temperature anisotropy A_{hp} = 2. The red dots represent the dimensionless maximum growth rates of the Alfvén-cyclotron instability derived from solving the kinetic linear dispersion equation, and the black curves correspond to the scaling of dimensionless maximum growth rates derived from Equation (3) with Equations (4a) and (4b).

Table 1. The fitting parameters h_1 and h_2 of Equation (3) as obtained from solutions of the linear dispersion relation for the maximum growth rates of the Alfvén-cyclotron instability for the parameters A_{hp} and β_{hp} as given.

		β_{hp} = 0.1	β_{hp} = 0.25	β_{hp} = 0.5	β_{hp} = 1.0	β_{hp} = 2.5	β_{hp} = 5.0
h_1	A_{hp} = 1	1.3090	1.3056	1.2595	1.2009	1.0994	0.9925
	A_{hp} = 2	1.2711	1.2054	1.1447	1.0643	0.9289	0.8005
	A_{hp} = 3	1.2032	1.1347	1.0630	0.9780	0.8323	0.7028
	A_{hp} = 4	1.1475	1.0786	1.0069	0.9185	0.7620	0.6380
h_2	A_{hp} = 1	1.3689	1.3854	1.4230	1.4758	1.5708	1.6510
	A_{hp}= 2	1.4142	1.4747	1.5248	1.5784	1.6689	1.7297
	A_{hp} = 3	1.4631	1.5284	1.5767	1.6418	1.7252	1.7696
	A_{hp} = 4	1.4918	1.5645	1.6213	1.6916	1.7644	1.7876

Equations (4a) and (4b) in the ranges $1 \le A_{hp} \le 4$ and $0.1 \le \beta_{hp} \le 5.0$ yield the following results:

$$\varepsilon_1 = -0.42,\ \varepsilon_{11} = 0.36,\ \varepsilon_{12} = 0.22,\ \varepsilon_{13} = 1.6;\ \varepsilon_2 = 1.5,\ \varepsilon_{21} = 0.08,\ \varepsilon_{22} = 0.05. \quad (5)$$

The black curves in Figure 2 demonstrate the scalings for the Alfvén-cyclotron instability when using Equation (3) with Equations (4a) and (4b). As shown in Figure 2, the dimensionless growth rates $\gamma_m/\gamma_{m,M}$ minimize at small κ-values. Subsequently, $\gamma_m/\gamma_{m,M}$ rises substantially and generally stabilizes at ~1 at large κ-values. As A_{hp} and β_{hp} increase, the dimensionless maximum growth rates at small κ-values undergo a significant increase, whereas those at large κ-values exhibit negligible responses to the variations in plasma parameters. When we compare the solutions to the kinetic linear dispersion equation with the scaled instability evaluated by Equation (3) for the temperature anisotropy and plasma beta values indicated, our fits present good agreement with the numerical solutions. Specifically, the scalings give the best performance for large κ-values, namely, $\kappa > 40$. In addition, the fitting tends to exhibit better consistency with numerical results for higher A_{hp} and β_{hp}. As illustrated in Figures 2a–2d, at A_{hp}= 1, the scaling slightly overestimates the numerical maximum growth rate at κ = 2, whereas for A_{hp}= 3, this overestimation is fixed. Our fits also replicate the numerical growth rates more accurately at intermediate κ-values (κ = ~5–40), but for κ = ~3–5, the fits become marginally greater than the numerical results at higher A_{hp}. Regardless of the A_{hp}, the scalings generally precisely model the numerical dimensionless maximum growth rates at a large spectral index. As for the dependence of scaling on the plasma beta, the results exhibit a pattern similar to that with A_{hp}.

Figure 3 displays the dimensionless maximum growth rates derived from the kinetic linear dispersion equation (symbols) and Equation (3) (dashed lines) as a function of plasma beta β_{hp} for the labeled spectral indexes. As shown in the figure, as β_{hp} increases, the dimensionless maximum growth rates increase steadily, showing a linear relation to β_{hp}. As the κ-value rises from 2 to 10, the enhancements corresponding to increasing β_{hp} generally slow down, with the slope of the red dashed lines declining to nearly 0. For increasing A_{hp} (i.e., Figures 3a–3d), the dimensionless maximum growth rates generally undergo an enhancement. For low β_{hp}, $\gamma_m/\gamma_{m,M}$ increases moderately for the growing temperature anisotropy, whereas for high β_{hp}, the increase becomes milder. Therefore, it results in a flatter curve that relates the dimensionless maximum growth rates to plasma beta at higher A_{hp}. For increasing κ-values, the enhancements of $\gamma_m/\gamma_{m,M}$ attributable to increasing A_{hp} generally diminish for all the indicated β_{hp}. Regarding the performance of our scalings, the fits slightly overestimate the growth rates at intermediate β_{hp}. However, the difference between the modeled results and the numerical solutions tends to dampen and become primarily consistent for higher A_{hp}. As for larger κ-values, the fits provide better efficiency in accurately modeling the numerical dimensionless maximum growth rates. Under all indicated A_{hp}, the scalings of the Alfvén-cyclotron instability generally present good agreement with solutions to the linear dispersion equation, with slightly better agreement at higher A_{hp}.

We investigate the performance of our fits in modeling numerical dimensionless maximum growth rates under different plasma beta values (Figures 4a–4d) with respect to the varying temperature anisotropy values for the four labeled spectral indexes in

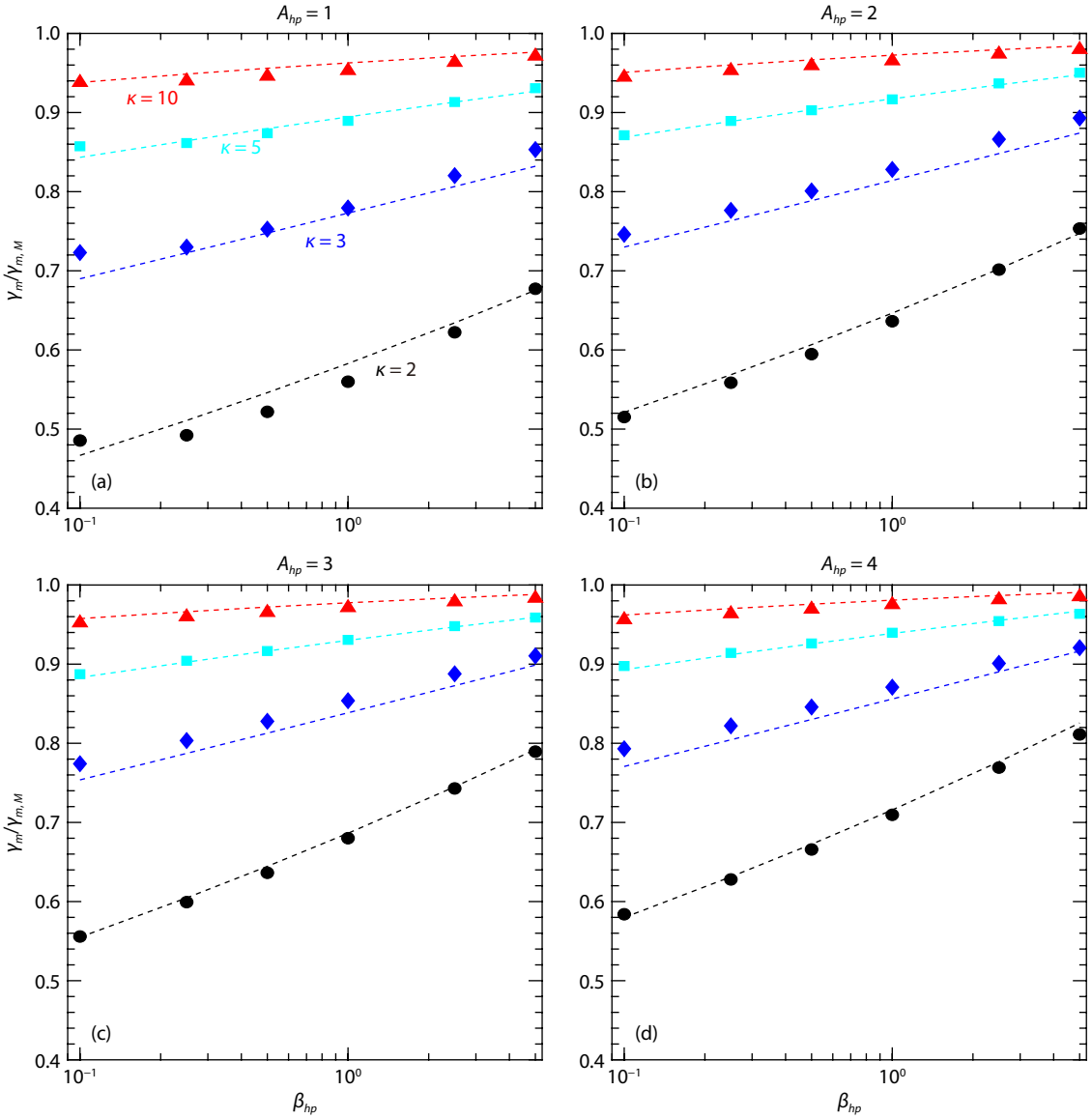

Figure 3. Normalized maximum growth rates as a function of plasma beta β_{hp} for different temperature anisotropy values (A_{hp} = 1, 2, 3, and 4, respectively). The symbols indicate solutions to the kinetic linear dispersion equation, and the dashed lines indicate the fitted growth rates evaluated by Equation (3). The black, blue, cyan, and red lines and symbols represent the results of the spectral index κ = 2, 3, 5, and 10, respectively.

Figure 4. Similar to Figure 3, as A_{hp} increases, $\gamma_m/\gamma_{m,M}$ increases substantially. Furthermore, for larger κ-values, $\gamma_m/\gamma_{m,M}$ becomes close to 1, with growth rates increasing more significantly at low A_{hp} and becoming milder for high A_{hp}. As β_{hp} increases, $\gamma_m/\gamma_{m,M}$ increases uniformly for different A_{hp}. For the fits, our results slightly overestimate the dimensionless maximum growth rates at $\kappa = 2$, which are subsequently corrected at higher β_{hp}. It is noteworthy that our fits generally accurately model the numerical dimensionless maximum growth rates, especially for large κ-values and high β_{hp}.

4. Discussion and Conclusions

In this study, our scaling formula provides the growth rate of the Alfvén-cyclotron instability in a bi-kappa plasma normalized to that in a Maxwellian distribution. Since Gary et al. (2017) yielded the growth rate in a Maxwellian distribution, the value of the Alfvén-cyclotron instability growth rate can be readily obtained by combining Equation (4) in our work and Equation (8) in Gary et al. (2017). Therefore, in an event study, the formula can be used to estimate the growth rate with only the measurements of plasma parameters (e.g., plasma beta, temperature anisotropy). Likewise, the formula can be used in large-scale models of the Earth's magnetosphere to provide global wave instability maps attributable to the Alfvén-cyclotron instability, which may help deepen the understanding of the statistical features of global wave distributions (i.e., for wave occurrence and strength, or others).

In addition to the temperature anisotropy and plasma beta, the fractional density of hot protons to the electron density N_{hp}/N_e is another important parameter that might significantly affect the

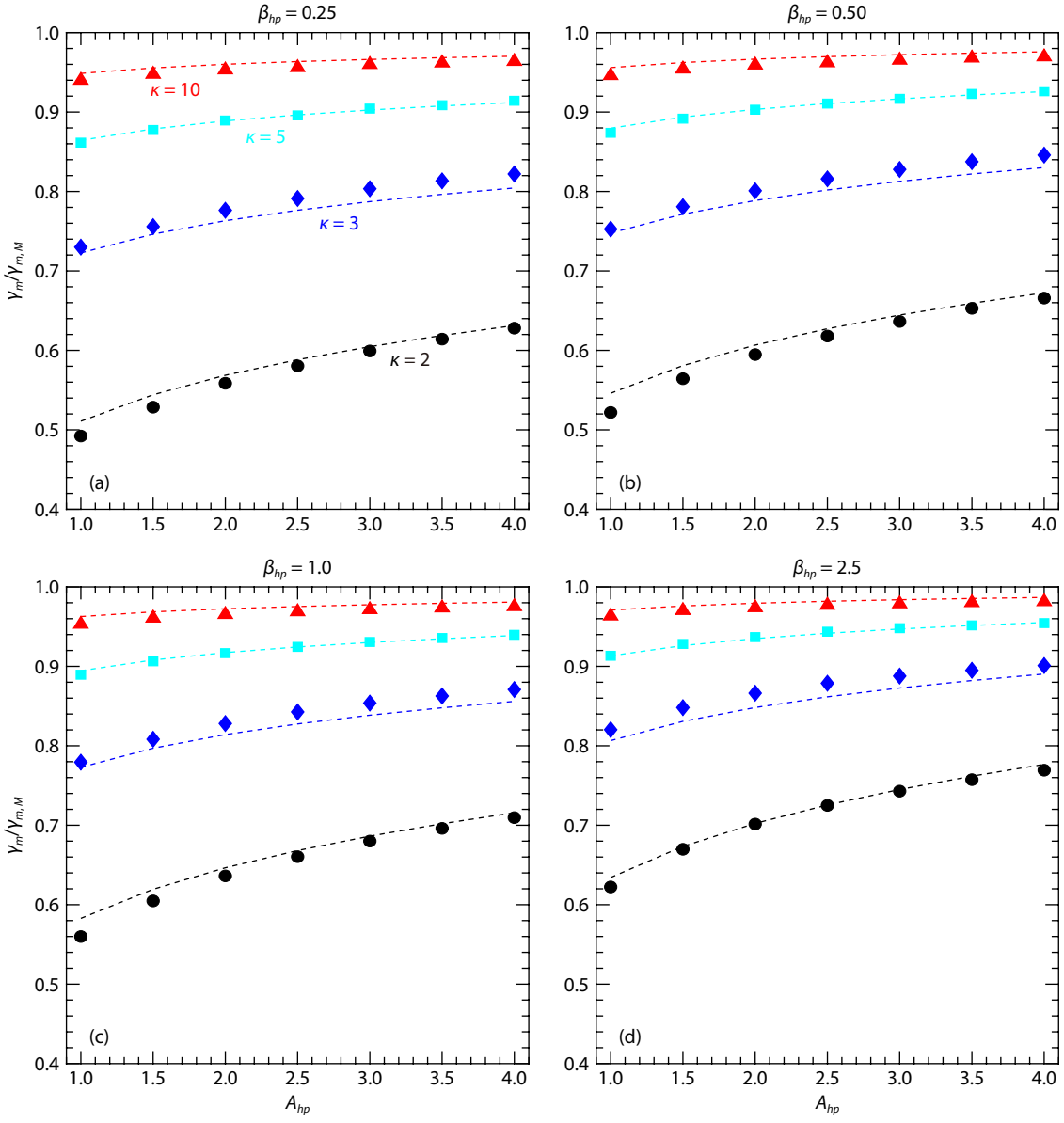

Figure 4. Normalized maximum growth rates as a function of temperature anisotropy A_{hp} for different plasma beta (β_{hp} = 0.25, 0.50, 1.0, and 2.5, respectively). The symbols indicate solutions to the kinetic linear dispersion equation, and the dashed lines indicate the fitted growth rates evaluated by Equation (3). The black, blue, cyan, and red lines and symbols represent the results of the spectral index κ = 2, 3, 5, and 10.

instability growth rates. Therefore, we investigate the sensitivity of dimensionless maximum growth rates to the hot proton abundance N_{hp}/N_e under different A_{hp} (Figures 5a–5d), and β_{hp} (Figures 5e–5f) at four specific spectral indexes κ = 2, 3, 5, 10 (represented by symbols in each subplot). Figure 5 shows that although $\gamma_m/\gamma_{m,M}$ undergoes a moderate increase with increasing plasma parameters A_{hp} and β_{hp}, the dimensionless maximum growth rates of the Alfvén-cyclotron instability are relatively insensitive to the variations in N_{hp}/N_e. Especially for a large κ-value (κ = 10), $\gamma_m/\gamma_{m,M}$ remains almost unchanged for increasing the abundance of hot protons. Consequently, in this study, for simplicity, the hot proton abundance is not incorporated into the scaling of the Alfvén-cyclotron instability.

Our adoption of purely hot protons, cold protons, and electrons for modeling the particle distributions in space plasma is an idealized assumption. Heavier ions, such as He^+ and O^+, occupy a nonnegligible portion of magnetospheric particles, and the abundance of heavy ions can be highly dynamic during geomagnetically active conditions. The presence of heavy ions and the variation in the ion compositions could dramatically modify the dispersion relation and corresponding growth rates of the Alfvén-cyclotron instability in a kappa plasma. Therefore, in the scaling of instability growth rates, we would consider incorporating the heavy ions and investigating the performance of our fits under different conditions of heavy ion abundance in a future study. In addition, because oblique EMIC waves are often observed and can significantly affect the particle scattering (Ni BB et al., 2015; Min K et al., 2016; Cao X et al., 2019), the scaling of oblique EMIC waves would be our future work.

In this study, by solving the kinetic linear dispersion equation in a bi-kappa plasma, we explore the response of Alfvén-cyclotron instability growth rates to variations in the spectral index of the bi-kappa distribution under different plasma conditions (i.e., the temperature isotropy and plasma beta of hot protons). Moreover, linear theory yields scaling relations for the dimensionless maximum growth rates. Our results indicate that as the κ-value increases, the instability bandwidth of the wave number narrows. To some extent, this result also represents a narrowing of the bandwidth of wave frequency spectra. In addition, the maximum growth rate increases monotonically with a rising κ-value. As β_{hp} and A_{hp} increase, the maximum growth rate undergoes a noticeable enhancement owing to more free energy contributed to driving the instability. Scaling relations are expressed by relatively concise, analytic formulas, which are functions of the spectral index κ and the temperature anisotropy A_{hp} and plasma beta β_{hp} of hot protons. The results show that our fits present good agreement with the numerical solutions to linear dispersion theory with acceptable error. The fits tend to overestimate the growth rates at small κ-values for low β_{hp} and A_{hp}, which are corrected at higher β_{hp} and A_{hp}. In general, our fits are capable of accurately modeling the numerical solutions, especially for large κ-values and high β_{hp} and A_{hp}.

In addition, similar to the excitation of Alfvén-cyclotron instability due to the proton temperature anisotropy, whistler waves are generally excited by the electron temperature anisotropy (Xiao F et al., 2006; Lu Q et al., 2010; Ni B et al., 2016). Previous studies show that in a kappa plasma, the increasing of spectral index κ and plasma beta of energetic electrons provide favorable conditions for the excitation of whistler waves (Xiao F et al., 2006; Lu Q et al., 2010). Compared with the excitation characteristics of whistler waves, the Alfvén-cyclotron instability exhibits a similar pattern of increasing growth rate for larger spectral indexes and

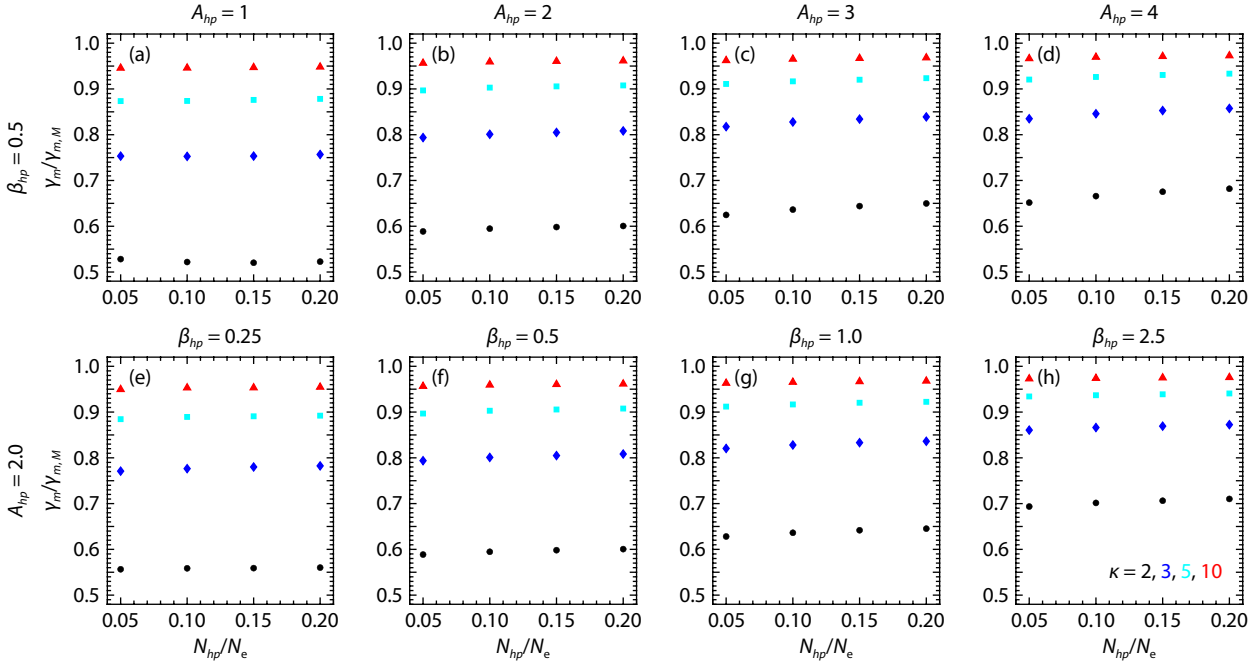

Figure 5. Dimensionless maximum growth rates as a function of hot proton abundance for (a–d) the four temperature anisotropy values indicated (A_{hp}=1, 2, 3, and 4) at a fixed plasma beta β_{hp}= 0.5, and (e–h) the four plasma beta values indicated (β_{hp} = 0.25, 0.50, 1.0, and 2.5) at a fixed temperature anisotropy A_{hp} = 2.

plasma beta of hot protons. However, as reported in Xiao F et al. (2006), the ratio of energetic electrons density over the total plasma density is important for the whistler mode wave growth, while the Alfvén-cyclotron instability is less sensitive to the variations of hot proton density.

Acknowledgments

This work was supported by the National Natural Science Foundation of China (Grant Nos. 42204163, 42188101, 42025404, 42241143, 41774167, 41774171, 41974205, 41804157, 41904156, 42130204, and 42241133), the B-type Strategic Priority Program of the Chinese Academy of Sciences (Grant No. XDB41000000), the National Key R&D Program of China (Grant Nos. 2022YFF0503700 and 2022YFF0503900), the pre-research projects on Civil Aerospace Technologies (Grant No. D020103) funded by the China National Space Administration, the Macau Foundation, the Fundamental Research Funds for the Central Universities (Grant No. 2042022kf1012), and the Shenzhen Key Laboratory Launching Project (Grant No. ZDSYS20210702140800001). TieLong Zhang was supported by the Chinese Academy of Sciences Center for Excellence in Comparative Planetology.

References

Blum, L. W., MacDonald, E. A., Gary, S. P., Thomsen, M. F., and Spence, H. E. (2009). Ion observations from geosynchronous orbit as a proxy for ion cyclotron wave growth during storm times. *J. Geophys. Res.*: *Space Phys.*, *114*(A10), A10214. https://doi.org/10.1029/2009JA014396

Bortnik, J., Omidi, N., Chen, L., Thorne, R. M., and Horne, R. B. (2011). Saturation characteristics of electromagnetic ion cyclotron waves. *J. Geophys. Res.*: *Space Phys.*, *116*(A9), A09219. https://doi.org/10.1029/2011JA016638

Cao, J. B., Duan, A. Y., Reme, H., and Dandouras, I. (2013). Relations of the energetic proton fluxes in the central plasma sheet with solar wind and geomagnetic activities. *J. Geophys. Res.*: *Space Phys.*, *118*(11), 7226–7236. https://doi.org/10.1002/2013JA019289

Cao, X., Ni, B. B., Liang, J., Xiang, Z., Wang, Q., Shi, R., Gu, X. D., Zhou, C., Zhao, Z. Y., … Liu, J. (2016). Resonant scattering of central plasma sheet protons by multiband EMIC waves and resultant proton loss timescales. *J. Geophys. Res.*: *Space Physics*, *121*(2), 1219–1232. https://doi.org/10.1002/2015JA021933

Cao, X., Shprits, Y. Y., Ni, B. B., and Zhelavskaya, I. S. (2017a). Scattering of ultra-relativistic electrons in the Van Allen radiation belts accounting for hot plasma effects. *Sci. Rep.*, *7*(1), 17719. https://doi.org/10.1038/s41598-017-17739-7

Cao, X., Ni, B. B., Summers, D., Bortnik, J., Tao, X., Shprits, Y. Y., Lou, Y. Q., Gu, X. D., Fu, S., … Wang, Q. (2017b). Bounce resonance scattering of radiation belt electrons by H^+ band EMIC waves. *J. Geophys. Res.*: *Space Phys.*, *122*(2), 1702–1713. https://doi.org/10.1002/2016JA023607

Cao, X., Ni, B. B., Summers, D., Shprits, Y. Y., Gu, X. D., Fu, S., Lou, Y. Q., Zhang, Y., Ma, X., … Yi, J. (2019). Sensitivity of EMIC wave-driven scattering loss of ring current protons to wave normal angle distribution. *Geophys. Res. Lett.*, *46*(2), 590–598. https://doi.org/10.1029/2018GL081550

Cao, X., Ni, B. B., Summers, D., Shprits, Y. Y., and Lou, Y. Q. (2020a). Effects of polarization reversal on the pitch angle scattering of radiation belt electrons and ring current protons by EMIC waves. *Geophys. Res. Lett.*, *47*(17), e2020GL089718. https://doi.org/10.1029/2020GL089718

Cao, X., Ni, B. B., Summers, D., Ma, X., Lou, Y. Q., Zhang, Y., Gu, X. D., and Fu, S. (2020b). Effects of superthermal plasmas on the linear growth of multiband EMIC waves. *Astrophy. J.*, *899*(1), 43. https://doi.org/10.3847/1538-4357/ab9ec4

Cao, X., Lu, P., Ni, B. B., Summers, D., Shprits, Y. Y., Long, M. Y., and Wang, X. Y. (2023). Resonant scattering of radiation belt electrons at Saturn by ion cyclotron waves. *Geophys. Res. Lett.*, *50*(3), e2022GL102394. https://doi.org/10.1029/2022GL102394

Chaston, C. C., Hu, Y. D., and Fraser, B. J. (1997). Non-Maxwellian particle distributions and electromagnetic ion cyclotron instabilities in the near-Earth magnetotail. *Geophys. Res. Lett.*, *24*(22), 2913–2916. https://doi.org/10.1029/97GL02972

Chen, H., Gao, X., Lu, Q., and Wang, S. (2018). In Situ Observations of Harmonic Alfvén Waves and Associated Heavy Ion Heating. *Astrophy. J.*, *859*(2), 120. https://doi.org/10.3847/1538-4357/aabee2

Christon, S. P., Mitchell, D. G., Williams, D. J., Frank, L. A., Huang, C. Y., and Eastman, T. E. (1988). Energy spectra of plasma sheet ions and electrons from ~50 eV/e to ~1 MeV during plasma temperature transitions. *J. Geophys. Res.*: *Space Phys.*, *93*(A4), 2562–2572. https://doi.org/10.1029/ja093ia04p02562

Cornwall, J. M. (1965). Cyclotron instabilities and electromagnetic emission in the ultra low frequency and very low frequency ranges. *J. Geophys. Res.*, *70*(1), 61–69. https://doi.org/10.1029/JZ070i001p00061

Cornwall, J. M., Coroniti, F. V., and Thorne, R. M. (1970). Turbulent loss of ring current protons. *J. Geophys. Res.*, *75*(25), 4699–4709. https://doi.org/10.1029/JA075i025p04699

Engebretson, M. J., Posch, J. L., Braun, D. J., Li, W., Ma, Q., Kellerman, A. C., Huang, C. L., Kanekal, S. G., Kletzing, C. A., … Ermakova, E. (2018). EMIC wave events during the four GEM QARBM challenge intervals. *J. Geophys. Res.*: *Space Phys.*, *123*(8), 6394–6423. https://doi.org/10.1029/2018JA025505

Fu, X. R., Cowee, M. M., Jordanova, V. K., Gary, S. P., Reeves, G. D., and Winske, D. (2016). Predicting electromagnetic ion cyclotron wave amplitude from unstable ring current plasma conditions. *J. Geophys. Res.*: *Space Phys.*, *121*(11), 10954–10965. https://doi.org/10.1002/2016JA023303

Gary, S. P. (1993). *Theory of Space Plasma Microinstabilities*. New York: Cambridge University Press. https://doi.org/10.1017/CBO9780511551512

Gary, S. P., Fu, X. R., Cowee, M. M., Winske, D., and Liu, K. J. (2017). Scalings for the Alfvén-cyclotron instability: linear dispersion theory and hybrid particle-in-cell simulations. *J. Geophys. Res.*: *Space Phys.*, *122*(1), 464–474. https://doi.org/10.1002/2016JA023425

Hao, Y. Q., Huang, J. P., Liu, W. L., Zhang, D. H., and Xiao, Z. (2017). Prompt GPS TEC response to magnetospheric compression. *J. Geophys. Res.*: *Space Phys.*, *122*(4), 4357–4366. https://doi.org/10.1002/2017JA023866

Kang, N., Lu, Q., Gao, X., Wang, X., Chen, H., and Wang, S. (2021). Propagation of electromagnetic ion cyclotron waves in a dipole magnetic field: A 2-D hybrid simulation. *J. Geophys. Res.*: *Space Physics*, *126*, e2021JA029720. https://doi.org/10.1029/2021JA02972

Kitamura, N., Kitahara, M., Shoji, M., Miyoshi, Y., Hasegawa, H., Nakamura, S., Katoh, Y., Saito, Y., Yokota, S., … Burch, J. L. (2018). Direct measurements of two-way wave–particle energy transfer in a collisionless space plasma. *Science*, *361*(6406), 1000–1003. https://doi.org/10.1126/science.aap8730

Liang, J., Donovan, E., Ni, B., Yue, C., Jiang, F., and Angelopoulos, V. (2014). On an energy-latitude dispersion pattern of ion precipitation potentially associated with magnetospheric EMIC waves. *J. Geophys. Res.*: *Space Phys.*, *119*(10), 8137–8160. https://doi.org/10.1002/2014JA020226

Liu, K. J., Gary, S. P., and Winske, D. (2010). Spectral properties of the Alfvén cyclotron instability: applications to relativistic electron scattering. *J. Geophys. Res.*: *Space Phys.*, *115*(A8), A08212. https://doi.org/10.1029/2009JA015201

Livadiotis, G. (2015). Introduction to special section on origins and properties of kappa distributions: statistical background and properties of kappa distributions in space plasmas. *J. Geophys. Res.*: *Space Phys.*, *120*(3), 1607–1619. https://doi.org/10.1002/2014JA020825

Lou, Y. Q., Cao, X., Ni, B. B., Wu, M. Y., and Zhang, T. L. (2021). Parametric dependence of polarization reversal effects on the particle pitch angle scattering by EMIC waves. *J. Geophys. Res.*: *Space Phys.*, *126*(12), e2021JA029966. https://doi.org/10.1029/2021JA029966

Lu, H. Y., Cao, J. B., Zhou, M., Fu, H. S., Nakamura, R., Zhang, T. L., Khotyaintsev, Y. V., Ma, Y. D., and Tao, D. (2013). Electric structure of dipolarization fronts associated with interchange instability in the magnetotail. *J. Geophys. Res.*: *Space Phys.*, *118*(10), 6019–6025. https://doi.org/10.1002/jgra.50571

Lu, Q., and Li, X. (2007). Heating of ions by low-frequency Alfven waves. *Phys. Plasmas*, *14*, 042303. https://doi.org/10.1063/1.2715569

Lu, Q., Zhou, L., and Wang, S. (2010). Particle-in-cell simulations of whistler waves excited by an electron κ distribution in space plasma. *J. Geophys. Res.*: *Space Physics, 115*(A2). https://doi.org/10.1029/2009ja014580

Ma, Q., Li, W., Yue, C., Thorne, R. M., Bortnik, J., Kletzing, C. A., Kurth, W. S., Hospodarsky, G. B., Reeves, G. D., and Spence, H. E. (2019). Ion heating by electromagnetic ion cyclotron waves and magnetosonic waves in the Earth's inner magnetosphere. *Geophys. Res. Lett.*, *46*, 6258–6267. https://doi.org/10.1029/2019GL083513

Meredith, N. P., Horne, R. B., Kersten, T., Fraser, B. J., and Grew, R. S. (2014). Global morphology and spectral properties of EMIC waves derived from CRRES observations. *J. Geophys. Res.*: *Space Phys.*, *119*(7), 5328–5342. https://doi.org/10.1002/2014JA020064

Min, K., Liu, K. J., and Peter Gary, S. (2016). Scalings of Alfvén-cyclotron and ion Bernstein instabilities on temperature anisotropy of a ring-like velocity distribution in the inner magnetosphere. *J. Geophys. Res.*: *Space Phys.*, *121*(3), 2185–2193. https://doi.org/10.1002/2015JA022134

Ni, B., Thorne, R. M., Zhang, X. J., Bortnik, J., Pu, Z. Y., Xie, L., Hu, Z. J., Han, D. S., Shi, R., … Gu, X. D. (2016). Origins of the Earth's diffuse auroral precipitation. *Space Sci. Rev.*, *200*(1-4), 205–259. https://doi.org/10.1007/s11214-016-0234-7

Ni, B. B., Cao, X., Zou, Z. Y., Zhou, C., Gu, X. D., Bortnik, J., Zhang, J. C., Fu, S., Zhao, Z. Y., … Xie, L. (2015). Resonant scattering of outer zone relativistic electrons by multiband EMIC waves and resultant electron loss time scales. *J. Geophys. Res.*: *Space Phys.*, *120*(9), 7357–7373. https://doi.org/10.1002/2015JA021466

Shprits, Y. Y. (2009). Potential waves for pitch-angle scattering of near-equatorially mirroring energetic electrons due to the violation of the second adiabatic invariant. *Geophys. Res. Lett.*, *36*(12), L12106. https://doi.org/10.1029/2009GL038322

Shprits, Y. Y., Drozdov, A. Y., Spasojevic, M., Kellerman, A. C., Usanova, M. E., Engebretson, M. J., Agapitov, O. V., Zhelavskaya, I. S., Raita, T. J., … Aseev, N. A. (2016). Wave-induced loss of ultra-relativistic electrons in the Van Allen radiation belts. *Nat. Commun.*, *7*, 12883. https://doi.org/10.1038/ncomms12883

Su, Z. P., Gao, Z. L., Zhu, H., Li, W., Zheng, H. N., Wang, Y. M., Wang, S., Spence, H. E., Reeves, G. D., … Wygant, J. R. (2016). Nonstorm time dropout of radiation belt electron fluxes on 24 September 2013. *J. Geophys. Res.*: *Space Phys.*, *121*(7), 6400–6416. https://doi.org/10.1002/2016JA022546

Summers, D., and Thorne, R. M. (1991). The modified plasma dispersion function. *Phys. Fluids B*: *Plasma Phys.*, *3*(8), 1835–1847. https://doi.org/10.1063/1.859653

Summers, D., and Thorne, R. M. (2003). Relativistic electron pitch-angle scattering by electromagnetic ion cyclotron waves during geomagnetic storms. *J. Geophys. Res.*: *Space Phys.*, *108*(A4), 1143. https://doi.org/10.1029/2002JA009489

Thorne, R. M., and Kennel, C. F. (1971). Relativistic electron precipitation during magnetic storm main phase. *J. Geophys. Res.*, *76*(19), 4446–4453. https://doi.org/10.1029/JA076i019p04446

Thorne, R. M., and Horne, R. B. (1997). Modulation of electromagnetic ion cyclotron instability due to interaction with ring current O^+ during magnetic storms. *J. Geophys. Res.*: *Space Phys.*, *102*(A7), 14155–14163. https://doi.org/10.1029/96JA04019

Xiao, F. L., Zhou, Q. H., Zheng, H. N., and Wang, S. (2006). Whistler instability threshold condition of energetic electrons by kappa distribution in space plasmas. *J. Geophys. Res.*, *111*, A08208. https://doi.org/10.1029/2006JA011612

Xiao, F. L., Zhou, Q. H., He, H. Y., Zheng, H. N., and Wang, S. (2007). Electromagnetic ion cyclotron waves instability threshold condition of suprathermal protons by kappa distribution. *J. Geophys. Res.*: *Space Phys.*, *112*(A7), A07219. https://doi.org/10.1029/2006JA012050

Xiao, F. L., Yang, C., Zhou, Q. H., He, Z. G., He, Y. H., Zhou, X. P., and Tang, L. J. (2012). Nonstorm time scattering of ring current protons by electromagnetic ion cyclotron waves. *J. Geophys. Res.*: *Space Phys.*, *117*(A8), A08204. https://doi.org/10.1029/2012JA017922

Xue, S., Thome, R. M., and Summers, D. (1996). Growth and damping of oblique electromagnetic ion cyclotron waves in the Earth's magnetosphere. *J. Geophys. Res.*: *Space Phys.*, *101*(A7), 15457–15466. https://doi.org/10.1029/96JA01088

Yu, J., Li, L. Y., Cui, J., Cao, J. B., Wang, J., He, Z. G., and Yang, J. (2020). Nonlinear interactions between relativistic electrons and EMIC waves in magnetospheric warm plasma environments. *J. Geophys. Res.*: *Space Phys.*, *125*(12), e2020JA028089. https://doi.org/10.1029/2020JA028089

Yu, Y. Q., Hosokawa, K., Ni, B. B., Jordanova, V. K., Miyoshi, Y., Cao, J. B., Tian, X. B., and Ma, L. X. (2022). On the importance of using event-specific wave diffusion rates in modeling diffuse electron precipitation. *J. Geophys. Res.*: *Space Phys.*, *127*(4), e2021JA029918. https://doi.org/10.1029/2021JA029918

Yue, C., Jun, C. W., Bortnik, J., An, X., Ma, Q. L., Reeves, G. D., Spence, H. E., Gerrard, A. J., Gkioulidou, M., … Kletzing, C. A. (2019). The relationship between EMIC wave properties and proton distributions based on Van Allen Probes observations. *Geophys. Res. Lett.*, *46*(8), 4070–4078. https://doi.org/10.1029/2019GL082633

Zhang, J. C., Kistler, L. M., Mouikis, C. G., Dunlop, M. W., Klecker, B., and Sauvaud, J. A. (2010). A case study of EMIC wave-associated He^+ energization in the outer magnetosphere: cluster and Double Star 1 observations. *J. Geophys. Res.*: *Space Phys.*, *115*(A6), A06212. https://doi.org/10.1029/2009JA014784

Zhou, Q. H., Xiao, F. L., Shi, J. K. and Tang, L. J. (2012). Instability and propagation of EMIC waves in the magnetosphere by a kappa distribution. *J. Geophys. Res.*: *Space Phys.*, *117*(A6), A06203. https://doi.org/10.1029/2011JA017296

Zhou, Q. H., Xiao, F. L., Yang, C., He, Y. H., and Tang, L. J. (2013). Observation and modeling of magnetospheric cold electron heating by electromagnetic ion cyclotron waves. *J. Geophys. Res.*: *Space Phys.*, *118*(11), 6907–6914. https://doi.org/10.1002/2013JA019263

Zhu, M. H., Yu, Y. Q., Tian, X. B., Shreedevi, P. R., and Jordanova, V. K. (2021). On the ion precipitation due to field line curvature (FLC) and EMIC wave scattering and their subsequent impact on ionospheric electrodynamics. *J. Geophys. Res.*: *Space Phys.*, *126*(3), e2020JA028812. https://doi.org/10.1029/2020JA028812